Appl. Math. Mech. -Engl. Ed., **41**(4), 667–680 (2020)

Applied Mathematics and Mechanics (English Edition)

https://doi.org/10.1007/s10483-020-2601-5

Boundary layer flow of Maxwell fluid due to torsional motion of cylinder: modeling and simulation*

M. KHAN[1], A. AHMED[1], J. AHMED[1,2,†]

1. Department of Mathematics, Quaid-i-Azam University, Islamabad 44000, Pakistan;
2. Department of Basic Sciences, University of Engineering and Technology, Taxila 47050, Pakistan

(Received Dec. 9, 2019 / Revised Feb. 2, 2020)

Abstract This paper investigates the boundary layer flow of the Maxwell fluid around a stretchable horizontal rotating cylinder under the influence of a transverse magnetic field. The constitutive flow equations for the current physical problem are modeled and analyzed for the first time in the literature. The torsional motion of the cylinder is considered with the constant azimuthal velocity E. The partial differential equations (PDEs) governing the torsional motion of the Maxwell fluid together with energy transport are simplified with the boundary layer concept. The current analysis is valid only for a certain range of the positive Reynolds numbers. However, for very large Reynolds numbers, the flow becomes turbulent. Thus, the governing similarity equations are simplified through suitable transformations for the analysis of the large Reynolds numbers. The numerical simulations for the flow, heat, and mass transport phenomena are carried out in view of the bvp4c scheme in MATLAB. The outcomes reveal that the velocity decays exponentially faster and reduces for higher values of the Reynolds numbers and the flow penetrates shallower into the free stream fluid. It is also noted that the phenomenon of stress relaxation, described by the Deborah number, causes to decline the flow fields and enhance the thermal and solutal energy transport during the fluid motion. The penetration depth decreases for the transport of heat and mass in the fluid with the higher Reynolds numbers. An excellent validation of the numerical results is assured through tabular data with the existing literature.

Key words torsional motion, Maxwell fluid, magnetic field, stretchable rotating cylinder, bvp4c scheme

Chinese Library Classification O361
2010 Mathematics Subject Classification 76A05, 76A10

1 Introduction

In the subject of fluid dynamics, the flow induced by stretching and rotating surfaces has attracted researchers to investigate its characteristics due to its diverse applications in engineering mechanism, such as wire drawing, glass fiber, hot rolling, and paper production. In a

* Citation: KHAN, M., AHMED, A., and AHMED, J. Boundary layer flow of Maxwell fluid due to torsional motion of cylinder: modeling and simulation. *Applied Mathematics and Mechanics* (*English Edition*), **41**(4), 667–680 (2020) https://doi.org/10.1007/s10483-020-2601-5

† Corresponding author, E-mail: j.ahmed@math.qau.edu.pk

wide range of applications, from shafts and axles to spinning projectiles, the flow over rotating cylinders is also critically important. Crane[1] was the first who inspected the flow induced by a stretching cylinder. Afterwards, many researchers investigated the flow phenomena over stretching surfaces[2–4]. Fang and Yao[5] studied the flow of viscous fluid over the stretching and rotating cylinder with the assumption of axisymmetric flow. They considered the rotation of the cylinder is constant because a constant rotation of the cylinder does not induce secondary axial flow. Flow of viscous fluid induced by a purely rotating cylinder was investigated by Sprague and Weidman[6]. Subhashini et al.[7] found dual solutions for the flow over a stretching sheet with thermal diffusivity. The boundary layer flow and heat transfer over an exponentially stretching sheet under the influence of magnetic field were numerically studied by Mukhopadhyay[8]. An analytical study was performed by Dandapat et al.[9] on the unsteady thin film flow of bi-viscosity fluid over a stretching sheet. Their solution revealed that in the comparison of Newtonian fluid and bi-viscosity fluid, the thin film is faster for bi-viscosity fluid. Ahmed et al.[10] carried out the numerical investigation of the thin film flow of the Maxwell nanofluid over a rotating disk in the unsteady state. The outcomes of this study showed that for higher values of the magnetic parameter, the film thickness reduces. In recent studies, the flow of Casson fluid over the swirling cylinder in axisymmetry and energy transports was analyzed by Javed et al.[11]. The viscous fluid impinging radially on the swirling cylinder was examined by Weidman[12].

In the subject of fluid dynamics, both Newtonian and non-Newtonian fluids have ubiquitous applications in natural settings and engineering, including materials, chemical, food, and geological processes. However, most researchers are interested in studying Newtonian fluids, e.g., Salman et al.[13] presented the review on the properties of flow phenomenon and heat transport in conventional fluids as well as nanofluids. Recently, the non-Newtonian fluid investigations have been more and more attractive due to the plenteous role of these fluids in the exposure to fossil fuels, factory waste transmission, and heat exchangers. Javed et al.[14] numerically investigated the flow of Eyring-Powell fluid induced above the stretching sheet. Despite the Newtonian fluids, there is no single mathematical relation for the non-Newtonian fluids that describe complex rheological characteristics of these liquids. Various mathematical models have been proposed in the literature by researchers to predict all flow features of non-linear liquids. Among these models, the Maxwell fluid model portrays the rheology of rate type viscoelastic fluids that exhibits stress relaxation phenomena. Shi and Tang[15] performed the simulation on the rheology of non-Newtonian fluids in channels by utilizing the lattice Boltzmann method. Heat transfer enhancement in the thin film non-Newtonian fluid with embedded graphene nanoparticles was reported by Sandeep and Malvandi[16]. Analysis on the entropy generation in the MHD flow of third grade fluid with convective heat transport at the surface of stretching sheet was performed by Rashidi et al.[17]. Their results revealed that higher values Prandtl number decreases the thermal boundary layer thickness. Devakar et al.[18] numerically studied the flow of non-Newtonian fluid through a square duct with fully developed conditions. They found that the fully developed velocity profile for a couple stress fluid model and the Jeffrey fluid model. Picchi et al.[19] presented the exact solution for the stratified flows of Newtonian and non-Newtonian fluids in channels. In this investigation, they used the exact solution to study the rheology of Carreau fluid on two phase flow features for both gas/liquid and liquid/liquid systems. The studies on the fluid flow with heat transport in various geometries can be seen in Refs. [20]–[22], revealing the importance of non-Newtonian fluid models.

The aforementioned studies motivate us to propose the mathematical model for the flow of the Maxwell fluid over the rotating stretchable cylinder. This work is basically the extension of the work of Fang and Yao[5]. The formulated partial differential equations (PDEs) which govern the flow induced by stretching and rotating the cylinder and energy transport phenomena simplified by utilizing the boundary layer theory. In view of suitable flow similarities, the governing PDEs are transformed into a system of ordinary non-linear differential equations.

The solution to these ordinary differential equations (ODEs) for flow and energy transport is acquired with the help of the built-in MATLAB numerical scheme, i.e., bvp4c. Finally, the results for this physical problem are presented graphically with detailed physical discussion.

2 Mathematical formulation

Consider the swirling flow of the Maxwell fluid over a stretchable rotating cylinder with the radius R_1 under the influence of a magnetic field. Suppose that the velocity field for flow is $\boldsymbol{V} = (u(z, r), v(z, r), w(z, r))$, where u, v, and w are components along z-, θ-, and r-axes, respectively, and $\boldsymbol{B} = (0, 0, B_0)$ is the applied magnetic field in the direction of r-axis. We assume that the cylinder is rotating with a constant speed around its axis and the stretching velocity of the cylinder is directly proportional to the axial distance. The temperature and concentration at the surface of the cylinder are assumed as T_w and C_w, respectively. The flow scheme is presented in Fig. 1.

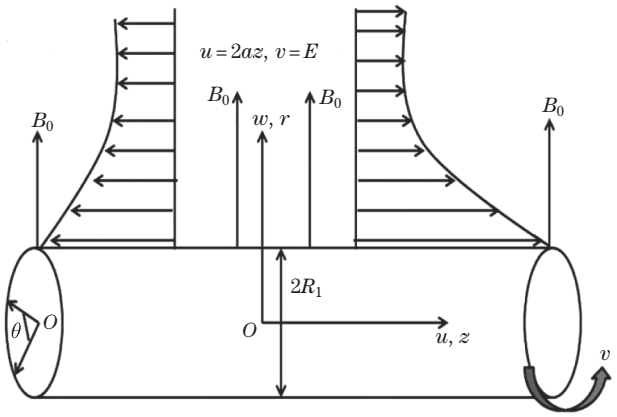

Fig. 1 Schematic diagram for flow configuration

The conservation laws for mass, momentum, and energy are defined as

$$\boldsymbol{\nabla} \cdot \boldsymbol{V} = 0, \tag{1}$$

$$\rho \frac{\mathrm{d}\boldsymbol{V}}{\mathrm{d}t} = -\boldsymbol{\nabla} p + \boldsymbol{\nabla} \cdot \boldsymbol{S} + \boldsymbol{J}_1 \times \boldsymbol{B}, \tag{2}$$

$$(\rho c_p) \frac{\mathrm{d}T}{\mathrm{d}t} = -\boldsymbol{\nabla} \cdot \boldsymbol{q}, \tag{3}$$

$$\frac{\mathrm{d}C}{\mathrm{d}t} = -\boldsymbol{\nabla} \cdot \boldsymbol{J}, \tag{4}$$

where $\frac{\mathrm{d}}{\mathrm{d}t}$ is the material derivative, ρ is the density of the fluid, p is the pressure, and $\boldsymbol{S}$ is the extra stress tensor, $\boldsymbol{J}_1$ is the current density, c_p is the specific heat capacity of the fluid at constant pressure, and $\boldsymbol{q}$ and $\boldsymbol{J}$ are the heat and mass fluxes which are defined from Fourier's and Fick's laws, respectively. The extra stress tensor for the Maxwell fluid is defined as

$$\left(1 + \lambda_1 \frac{\mathrm{D}}{\mathrm{D}t}\right) \boldsymbol{S} = \mu \boldsymbol{A}_1, \tag{5}$$

where λ_1 is the relaxation time, $\frac{\mathrm{D}}{\mathrm{D}t}$ signifies the Oldroyd derivative, $\boldsymbol{A}_1 = \boldsymbol{\nabla V} + (\boldsymbol{\nabla V})^{\mathrm{T}}$ is the first Rivlin-Ericksen tensor, and μ is the viscosity of the fluid. We can recover the Newtonian fluid case if $\lambda_1 = 0$. Based on the axisymmetric, steady, and incompressible assumptions and

by using the above equations and eliminating $\boldsymbol{S}$ in Eqs. (2) and (5), we obtain the governing boundary layer PDEs for the present flow and energy transport problem as follows:

$$\frac{\partial u}{\partial z}+\frac{w}{r}+\frac{\partial w}{\partial r}=0, \tag{6}$$

$$u\frac{\partial u}{\partial z}+w\frac{\partial u}{\partial r}+\lambda_1\Big(u^2\frac{\partial^2 u}{\partial z^2}+2uw\frac{\partial^2 u}{\partial r\partial z}+w^2\frac{\partial^2 u}{\partial r^2}\Big)$$
$$=-\frac{1}{\rho}\frac{\partial p}{\partial z}+v\Big(\frac{\partial^2 u}{\partial r^2}+\frac{1}{r}\frac{\partial u}{\partial r}\Big)-\frac{\sigma B_0^2}{\rho}\Big(u+\lambda_1 w\frac{\partial u}{\partial r}\Big), \tag{7}$$

$$u\frac{\partial v}{\partial z}+w\frac{\partial v}{\partial r}+\frac{wv}{r}+\lambda_1\Big(u^2\frac{\partial^2 v}{\partial z^2}+2uw\frac{\partial^2 v}{\partial r\partial z}+w^2\frac{\partial^2 v}{\partial r^2}+\frac{2wv}{r}\frac{\partial w}{\partial r}+\frac{2uv}{r}\frac{\partial w}{\partial z}-\frac{2w^2 v}{r^2}\Big)$$
$$=v\Big(\frac{\partial^2 v}{\partial r^2}-\frac{v}{r^2}+\frac{1}{r}\frac{\partial v}{\partial r}\Big)-\frac{\sigma B_0^2}{\rho}\Big(v+\lambda_1 w\frac{\partial v}{\partial r}-\lambda_1\frac{wv}{r}\Big), \tag{8}$$

$$u\frac{\partial T}{\partial z}+w\frac{\partial T}{\partial r}=\alpha_1\frac{1}{r}\frac{\partial}{\partial r}\Big(r\frac{\partial T}{\partial r}\Big), \tag{9}$$

$$u\frac{\partial C}{\partial z}+w\frac{\partial C}{\partial r}=D_B\frac{1}{r}\frac{\partial}{\partial r}\Big(r\frac{\partial C}{\partial r}\Big), \tag{10}$$

and the corresponding boundary conditions for the given flow problem are

$$\begin{cases} u(z,\,r)=2az, \quad v(z,\,r)=E, \quad w(z,\,r)=0, \quad T=T_{\rm w}, \quad C=C_{\rm w} \quad \text{at} \quad r=R_1,\\ u\to 0, \quad v\to 0, \quad T\to T_\infty, \quad C\to C_\infty \quad \text{as} \quad r\to\infty, \end{cases} \tag{11}$$

where v is the kinematic viscosity, α_1 and D_B are the thermal and mass diffusivities, respectively, $a>0$ having dimension T^{-1} describes the stretching strength of the cylinder, and E represents the constant torsional motion of the cylinder and its dimension is the same as the velocity.

The governing equations can be reduced to ODEs with the help of the following transformation group:

$$\begin{cases} u=2azf'(\eta), \quad v=Eg(\eta), \quad w=-aR_1\dfrac{f(\eta)}{\eta^{1/2}},\\ \theta(\eta)=\dfrac{T-T_\infty}{T_{\rm w}-T_\infty}, \quad \phi(\eta)=\dfrac{C-C_\infty}{C_{\rm w}-C_\infty}, \quad \eta=\dfrac{r^2}{R_1^2}. \end{cases} \tag{12}$$

After substituting the overhead ansatz, Eq. (6) is satisfied automatically, and Eqs. (7)–(11) yield

$$\eta f'''+f''+Reff''-Ref'^2-\beta_1 Re\Big(\frac{f^2 f''}{\eta}+2f^2 f'''-4ff'f''\Big)$$
$$-MRe\Big(\frac{f'}{2}-\beta_1 ff''\Big)=0, \tag{13}$$

$$2\eta^2 g''+2\eta g'-\frac{g}{2}+2Re\eta fg'+Refg-\beta_1 Re\Big(2f^2 g'+4\eta f^2 g''+4ff'g-\frac{4f^2 g}{\eta}\Big)$$
$$-MRe\Big(g-2\beta_1 fg'-\beta_1\frac{fg}{\eta}\Big)=0, \tag{14}$$

$$\eta\theta''+\theta'+RePrf\theta'=0, \tag{15}$$

$$\eta\phi''+\phi'+RePrLef\phi'=0 \tag{16}$$

with the boundary conditions

$$f(1)=0, \quad f'(1)=1, \quad g(1)=1, \quad \theta(1)=1, \quad \phi(1)=1, \tag{17}$$

$$f'(\infty)=0, \quad g(\infty)=0, \quad \theta(\infty)=0, \quad \phi(\infty)=0, \tag{18}$$

where $\beta_1 = \lambda_1 a$ is the Maxwell number, $Re = \frac{aR_1^2}{2\nu}$ is the Reynolds number, $M = \frac{\sigma B_0^2}{\rho a}$ is the magnetic parameter, $Pr = \frac{\nu}{\alpha_1}$ is the Prandtl number, and $Le = \frac{\alpha_1}{D_B}$ is the Lewis number. The above similar equations are valid for any positive values of Re and β_1. As reported by Fang and Yao[5] in the investigation of viscous flow due to the stretching and rotating cylinder, the solution convergence of flow equations is too slow, particularly for lower values of Re. Thus, following the Fang's work to make convergence fast, the variable η is transformed as $\eta = \mathrm{e}^x$. Then, Eqs. (13)–(18) become

$$
\begin{aligned}
&f_{xxx} - 2f_{xx} + f_x - Re(f_x^2 - ff_{xx} + ff_x) \\
&- \beta_1 Re\,\mathrm{e}^{-x}(2f^2 f_{xxx} - 5f^2 f_{xx} + 3f^2 f_x - 4ff_x f_{xx} + 4ff_x^2) \\
&- MRe\Big(\mathrm{e}^x \frac{f_x}{2} - \beta_1 ff_{xx} + \beta_1 ff_x\Big) = 0, \qquad (19)\\
&2g_{xx} - \frac{g}{2} + Re(2fg_x + fg) - \beta_1 Re\,\mathrm{e}^{-x}(6f^2 g_x + 4f^2 g_{xx} + 4ff_x g - 4f^2 g) \\
&- MRe(g - 2\beta_1 \mathrm{e}^{-x} fg_x - \beta_1 \mathrm{e}^{-x} fg) = 0, \qquad (20)\\
&\theta_{xx} + RePrf\theta_x = 0, \qquad (21)\\
&\phi_{xx} + RePrLe\phi_x = 0 \qquad (22)
\end{aligned}
$$

with the transformed boundary conditions

$$
\begin{aligned}
&f(0) = 0, \quad f_x(0) = 1, \quad g(0) = 1, \quad \theta(0) = 1, \quad \phi(0) = 1, \qquad (23)\\
&\lim_{x\to\infty} \mathrm{e}^{-x} f_x = 0, \quad g(\infty) = 0, \quad \theta(\infty) = 0, \quad \phi(\infty) = 0, \qquad (24)
\end{aligned}
$$

where the subscript x represents the derivative with respect to x.

2.1 Analysis for large Re

Before finding the numerical solution to the above ordinary differential system, we define the certain transformations for the simplification of the above equations to find the results for very large Re. Thus, the following transformations $\xi = \sqrt{Re}(\eta - 1), f(\eta) = \frac{1}{\sqrt{Re}} F(\xi)$, $g(\eta) = G(\xi), \theta(\eta) = \Theta(\xi)$, and $\phi(\eta) = \Phi(\xi)$ are substituted into Eqs. (19)–(24). Employing the limit $Re \to \infty$, we get

$$
\begin{aligned}
&F''' - F'^2 + FF'' - \beta_1(2F^2 F''' - 4FF'F'') - M\Big(\frac{F'}{2} - \beta_1 FF''\Big) = 0, \qquad (25)\\
&G'' + FG' - 2\beta_1 FG'' - M\Big(\frac{G}{2} - \beta_1 FG'\Big) = 0, \qquad (26)\\
&\Theta'' + PrF\Theta' = 0, \qquad (27)\\
&\Phi'' + PrLeF\Phi' = 0 \qquad (28)
\end{aligned}
$$

with the boundary conditions

$$
\begin{aligned}
&F(0) = 0, \quad F'(0) = 1, \quad G(0) = 1, \quad \Theta(0) = 1, \quad \Phi(0) = 1, \qquad (29)\\
&F(\infty) = 0, \quad G(\infty) = 0, \quad \Theta(\infty) = 0, \quad \Phi(\infty) = 0, \qquad (30)
\end{aligned}
$$

where the prime denotes the derivative with respect to ξ. Equation (25) corresponds to the flow problem for the Maxwell fluid over the stretching surface. This result is not unexpected and physically justified, because for very large Re, the curvature of the cylinder becomes very small and occupies the whole space, and it looks like a sheet. Moreover, for $\beta_1 = M = 0$, Eq. (25) reduces to the viscous fluid flow problem over the stretching sheet which was discussed by Wang[2].

2.1.1 Quantities of interest

The Nusselt and Sherwood numbers (Nu, Sh) are defined as

$$Nu = \frac{R_1 q_{\rm s}}{k(T_{\rm w} - T_\infty)}, \quad Sh = \frac{R_1 j_{\rm s}}{D_B(C_{\rm w} - C_\infty)}, \tag{31}$$

where $q_{\rm s}$ and $j_{\rm s}$ are the heat and mass fluxes, respectively,

$$q_{\rm s} = -k\Big(\frac{\partial T}{\partial r}\Big)_{r=R_1}, \quad j_{\rm s} = -D_B\Big(\frac{\partial C}{\partial r}\Big)_{r=R_1}. \tag{32}$$

The dimensionless form of Eq. (31) is given by

$$Nu = -2\theta'(1), \quad Sh = -2\phi'(1). \tag{33}$$

3 Numerical solution

This section is proposed for the numerical solution to the established ODEs for flow, energy, and concentration equations (19)–(22) along with the corresponding boundary conditions given in Eqs. (23) and (24). Furthermore, the numerical scheme is also employed for the solution to resulting Eqs. (25)–(28) in the analysis of the large Reynolds numbers with boundary conditions given in Eqs. (29) and (30). The built-in MATLAB technique named as bvp4c is used to acquire the numerical results. For this aim, we transform the governing ODEs to the system of the first-order ODEs. Thus, we use the transformed variables for Eqs. (19)–(22) as

$$f = y_1, \quad f_x = y_2, \quad f_{xx} = y_3, \quad f_{xxx} = yy_1, \tag{34}$$
$$g = y_4, \quad g_x = y_5, \quad g_{xx} = yy_2, \tag{35}$$
$$\theta = y_6, \quad \theta_x = y_7, \quad \theta_{xx} = yy_3, \tag{36}$$
$$\phi = y_8, \quad \phi_x = y_9, \quad \phi_{xx} = yy_4, \tag{37}$$

and for Eqs. (25)–(28) as

$$F = x_1, \quad F' = x_2, \quad F'' = x_3, \quad F''' = xx_1, \tag{38}$$
$$G = x_4, \quad G' = x_5, \quad G'' = xx_2, \tag{39}$$
$$\Theta = x_6, \quad \Theta' = x_7, \quad \Theta'' = xx_3, \tag{40}$$
$$\Phi = x_8, \quad \Phi' = x_9, \quad \Phi'' = xx_4. \tag{41}$$

The resulting first-order ODEs are

$$\begin{aligned} yy_1 &= 2y_3 - y_2 + Re(y_2^2 - y_1y_3 + y_1y_2) + \beta_1 Re\,{\rm e}^{-x}(3y_1^2y_2 - 5y_1^2y_3 - 4y_1y_2y_3 + 4y_1y_2^2) \\ &\quad + MRe\Big(\frac{{\rm e}^x y_2}{2} - \beta_1 y_1y_3 + \beta_1 y_1y_2\Big)\Big/a_1, \end{aligned} \tag{42}$$

$$\begin{aligned} yy_2 &= \frac{y_4}{2} - 2Rey_1y_5 - Rey_1y_4 + \beta_1 Re\,{\rm e}^{-x}(6y_1^2y_5 + 4y_1y_2y_4 - 4y_1^2y_4) \\ &\quad + MRe\Big(y_4 - 2\beta_1{\rm e}^{-x}y_1y_5 - \beta_1{\rm e}^{-x}y_1y_4\Big)\Big/a_2, \end{aligned} \tag{43}$$

$$yy_3 = -RePry_1y_7, \tag{44}$$

$$yy_4 = -ReLePry_1y_9, \tag{45}$$

where

$$a_1 = 1 - 2\beta_1 Re\,{\rm e}^{-x}y_1^2, \quad a_2 = 2 - 4\beta_1 Re\,{\rm e}^{-x}y_1^2, \tag{46}$$

and the corresponding boundary conditions for the above first-order differential system are

$$y_1(0) = 0, \quad y_2(0) = 1, \quad y_4(0) = 1, \quad y_6(0) = 1, \quad y_8(0) = 1, \tag{47}$$

$$\lim_{x\to\infty} \mathrm{e}^{-x} y_2 = 0, \quad y_4(\infty) = 0, \quad y_6(\infty) = 0, \quad y_8(\infty) = 1. \tag{48}$$

The conversions of Eqs. (25)–(28) into the first-order ODEs are obtained as

$$xx_1 = \frac{x_2^2 - x_1 x_3 - 4\beta_1 x_1 x_2 x_3 + M(\frac{x_2}{2} - \beta_1 x_1 x_3)}{b_1}, \tag{49}$$

$$xx_2 = \frac{M(\frac{x_4}{2} - \beta_1 x_1 x_5) - x_1 x_5}{b_1}, \tag{50}$$

$$xx_3 = -Pr x_1 x_7, \tag{51}$$

$$xx_4 = -LePr x_1 x_9, \tag{52}$$

where $b_1 = 1 - 2\beta_1 x_1^2$, and the boundary conditions for the above non-linear first-order differential system are

$$x_1(0) = 0, \quad x_2(0) = 1, \quad x_4(0) = 1, \quad x_6(0) = 1, \quad x_8(0) = 1, \tag{53}$$

$$x_2(\infty) = 0, \quad x_4(\infty) = 0, \quad x_6(\infty) = 0, \quad x_8(\infty) = 1. \tag{54}$$

4 Results

The physical analysis of graphical outcomes for flow velocity and thermal and solutal energy transports is presented in this part of the research work. The influence of pertinent parameters on the velocity, temperature, and concentration fields is presented graphically with the comparison of Newtonian and non-Newtonian fluids and $Re = 1$ and $Re = 3$. The values of the pertinent parameters are taken to be fixed as $\beta_1 = 0.5, M = 1, Pr = 6.5$, and $Le = 6.5$. It is found that the velocity of the fluid decays quickly to free stream for Newtonian fluid and large values of Reynolds number, and thus the flow produces only near to the surface of the cylinder. Furthermore, the heat and mass transport is higher in non-Newtonian fluid and at low Reynolds number. One thing should be noted here is that for $Re = 0$, the swirl velocity is independent of the axial velocity. Thus, from Eq. (14), we obtain the swirl velocity as $g(\eta) = \eta^{-1/2}$. Physically, for zero Reynolds number, the stretching of cylinder diminishes and the flow around the cylinder is due to the pure rotational constant motion. Moreover, the constant swirling motion of the cylinder does not induce a secondary axial flow of fluid.

The axial velocity fields for the increasing values of the Maxwell parameter β_1, Reynolds number Re, and magnetic parameter M are illustrated in Fig. 2. The results reveal that the axial velocity declines and decays exponentially for all of these three parameters. Figure 3 shows that the swirl velocity decreases for higher values of β_1, Re, and M. Moreover, the same result is true for the radial velocity which is portrayed in Fig. 4. The above results are physically valid, since higher values of the magnetic parameter M boost up the Lorentz force that occurs in the fluid flow due to the transverse applied magnetic field and provides the resistance to the flow velocity. Hence, in the results, the velocity of fluid decreases. In the case of higher values of the Maxwell parameter β_1, the stress relaxation phenomenon increases in viscoelastic fluid and the liquid becomes more solid-like for the fluid motion declines. The Reynolds number is the controlling parameter for the flow of the Maxwell fluid. Basically, Re is the ratio of the inertial force due to the surface stretching to the viscous force. Thus, the higher values of Re increase the inertial force in the system which opposes the fluid accelerating force. In consequence of this argument, the flow field decreases.

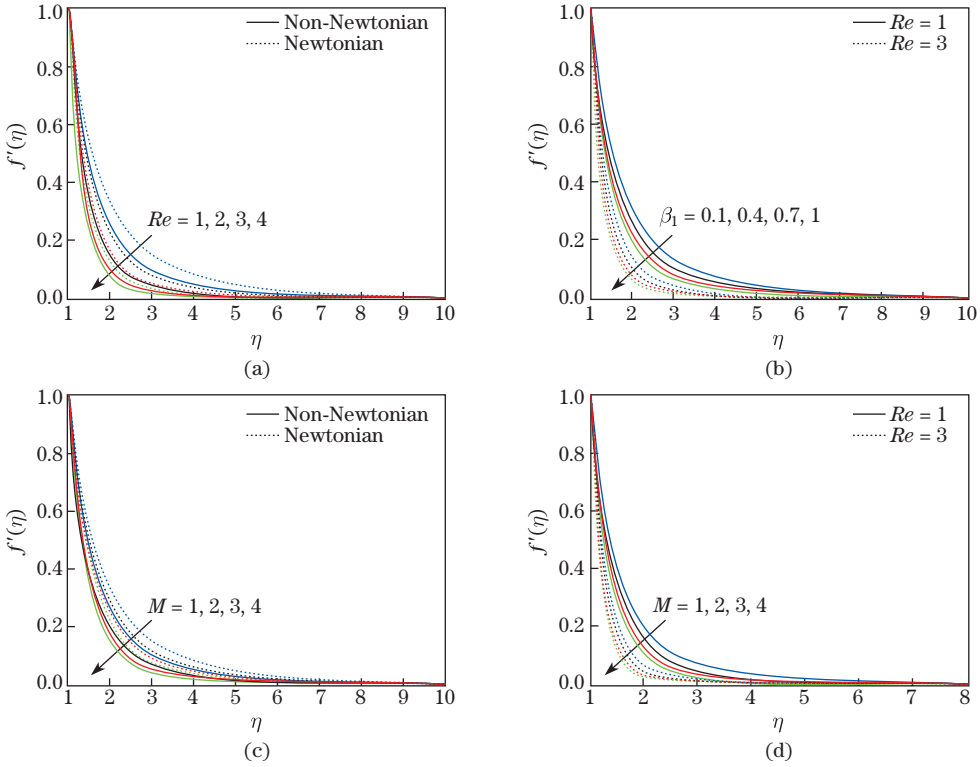

Fig. 2 Axial velocity profiles via Re, β_1, and M (color online)

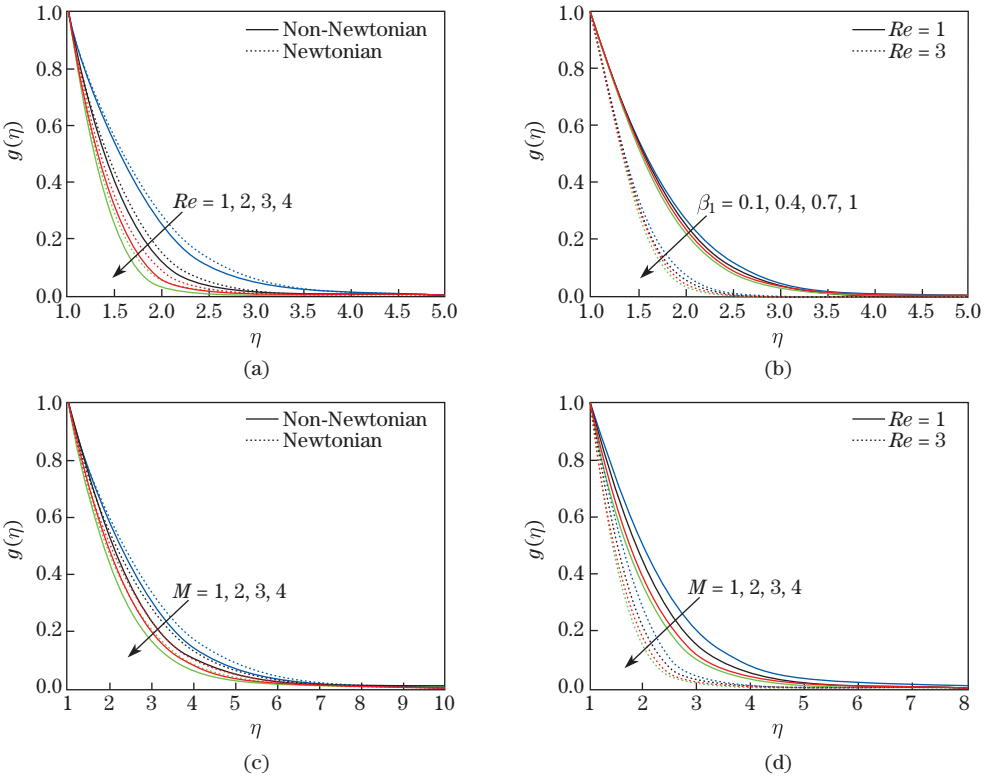

Fig. 3 Swirl velocity profiles via Re, β_1, and M (color online)

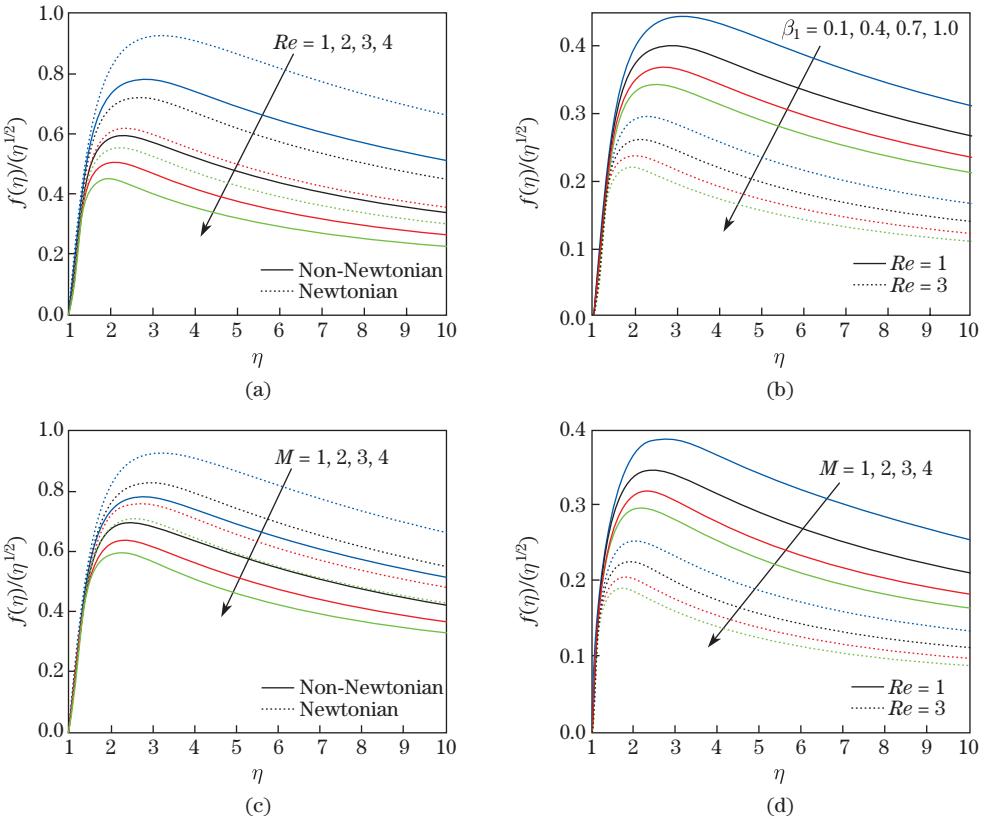

Fig. 4 Radial velocity profiles via Re, β_1, and M (color online)

The transport of thermal and solutal energy in the given swirling flow mechanism is visualized in Figs. 5 and 6. These graphical results for the temperature field prove that the higher values of the Maxwell parameter β_1 enhance the heat and mass transport rates in the flow. As mentioned above, for the larger values of β_1, the fluid behavior is solid-like, and thus particles of fluids are close to each other. As a consequence, the conduction of thermal and solutal energy boosts up in the fluid. The impact of Reynolds number Re on temperature and concentration profiles is found in decreasing trend. Physically, the Reynolds number controls the flow of fluid, and it is clear that higher values of Re reduce the flow field. Thus, the main forced convection mechanism for the transport of energy reduces. Therefore, the temperature and concentration fields decline. Moreover, the Prandtl number Pr and the Lewis number Le describe the relative importance of thermal and solutal energy transports in the fluid to the momentum transport. The higher values of both dimensionless numbers Pr and Le lower the temperature and concentration fields due to the reduction in the thermal and mass diffusivities of the fluid, respectively.

In the flow analysis for very large Reynolds number Re, Figs. 7 and 8 express the graphical results for the axial and swirl velocity fields, respectively, for increasing values of the Maxwell parameter β_1 and the magnetic parameter M. These findings reveal that the axial and swirl flow velocities decline. There is a same physical justification for this reduction in axial and swirl velocities, which is given above in cases of higher values of β_1 and M.

The physical mechanism for the transport of energy in the swirling flow of the Maxwell fluid for very large Reynolds number can be analyzed through the graphical outcomes given in Figs. 9 and 10. It can be seen that both thermal and solutal energy transports boost up for the increasing values of β_1 and M. Physically, in the case of higher magnetic parameter M, the

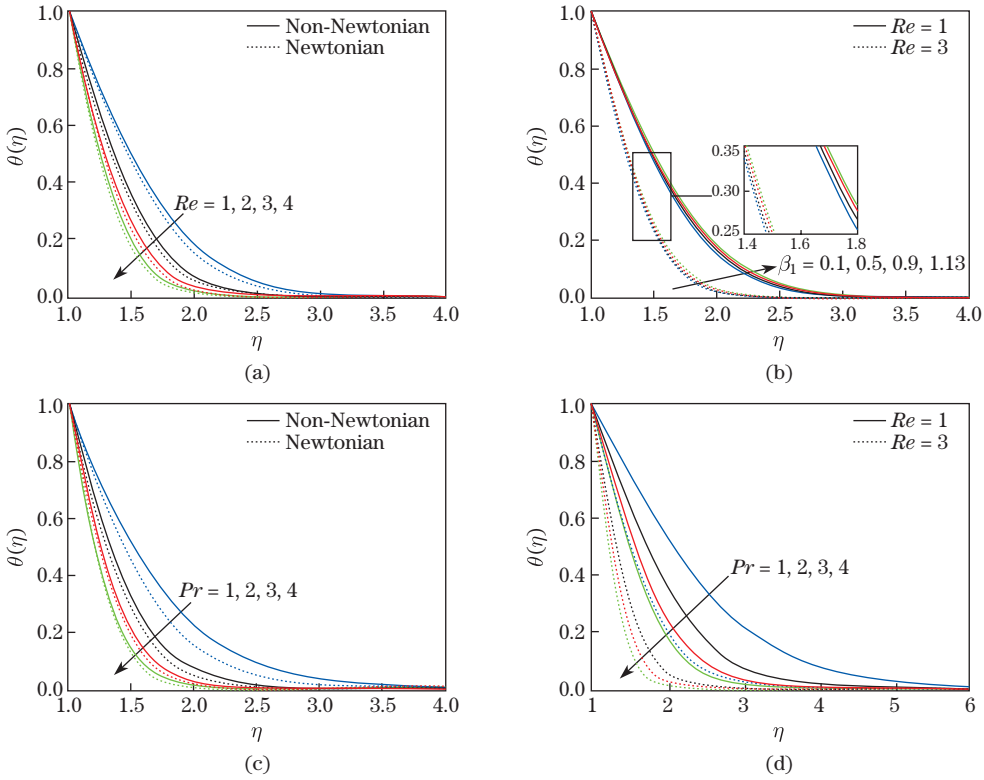

Fig. 5 Temperature profiles via Re, β_1, and Pr (color online)

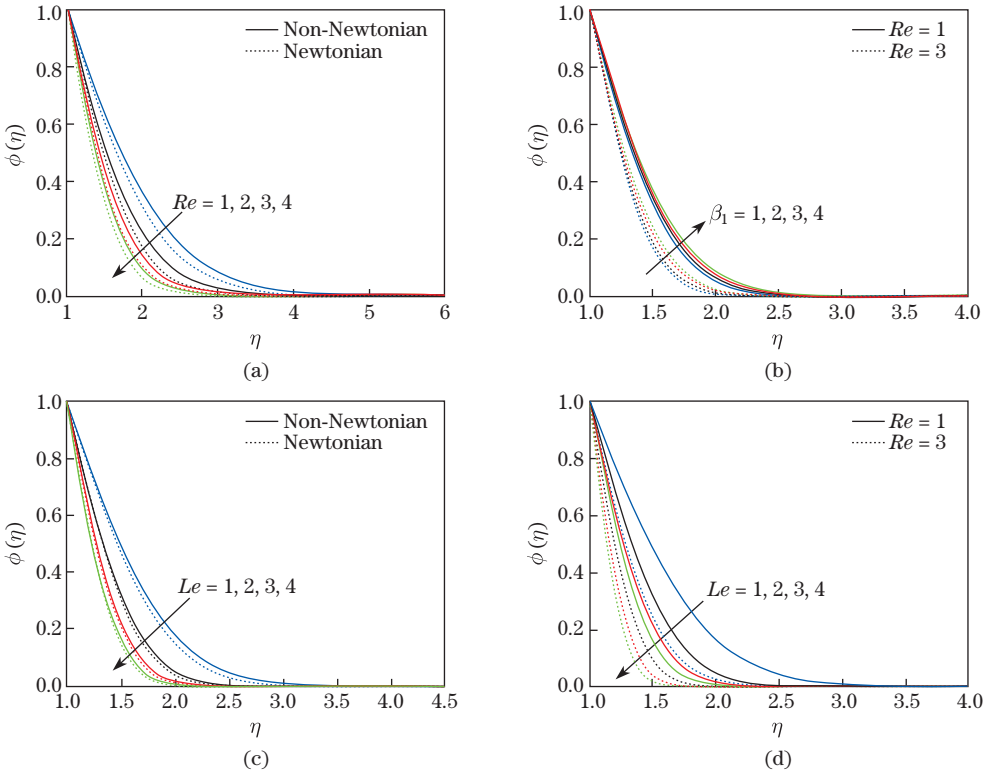

Fig. 6 Concentration profiles via Re, β_1, and Le (color online)

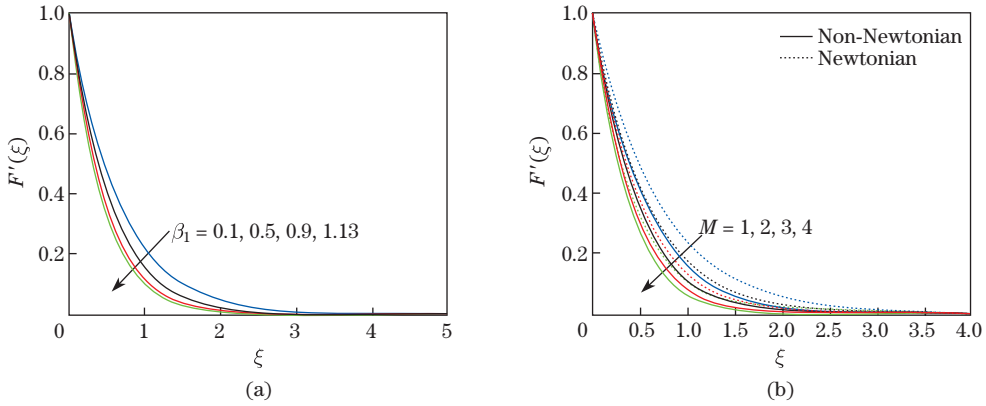

Fig. 7 Axial velocity profiles via (a) β_1 and (b) M for $Re \to \infty$ (color online)

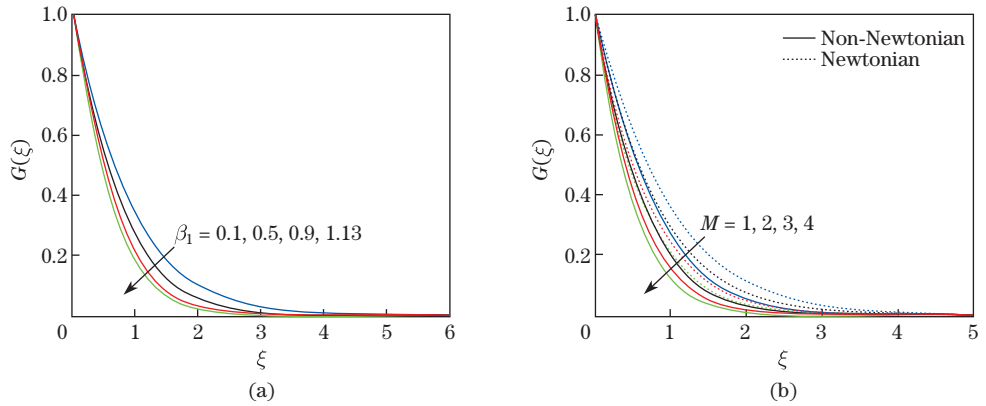

Fig. 8 Swirl velocity profiles via (a) β_1 and (b) M for $Re \to \infty$ (color online)

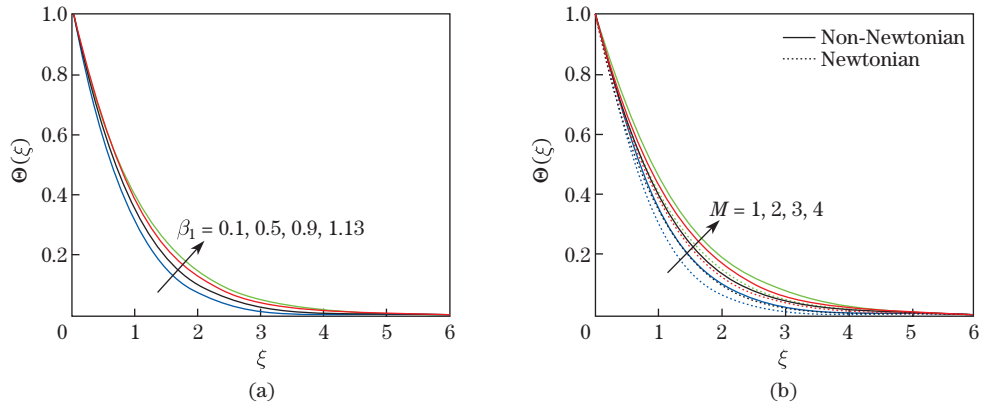

Fig. 9 Temperature profiles via (a) β_1 and (b) M for $Re \to \infty$ (color online)

conduction of energy increases between the fluid particles due to the enhancement in the Lorentz force. Here, we observe the same trends as in the case of β_1. Furthermore, in the comparison of Newtonian and non-Newtonian fluids for higher values of the magnetic parameter M, higher fluid flow velocity and less energy transport are observed for Newtonian fluids, and opposite trends are noted for non-Newtonian fluids.

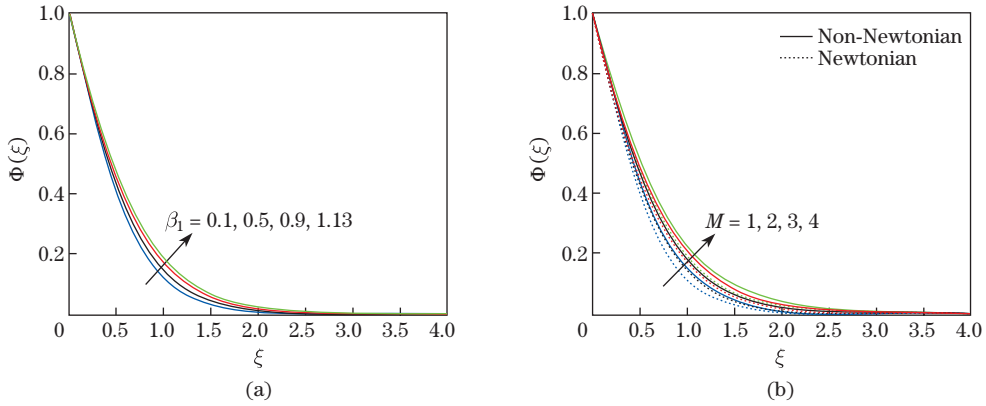

Fig. 10 Concentration profiles via (a) β_1 and (b) M for $Re \to \infty$

The comparison of the numerical values of the initial axial and swirl velocity gradients with existing articles for various values of Re is presented in Table 1. It is noted that the magnitude of these velocities gradients increases with the higher trend in Re. The numerical values of the Nusselt and Sherwood numbers are given in Table 2 for different pertinent parameters and fixed $M = 0$.

Table 1 A comparison of the axial and swirl velocity gradients for various values of Re in limiting case when $\beta_1 = M = Pr = Le = 0$

Re	Ref. [5]		Present result	
	$f''(1)$	$g'(1)$	$f''(1)$	$g'(1)$
0.1	−0.481 80	−0.510 19	−0.489 603	−0.510 233
0.2	−0.617 48	−0.526 05	−0.614 250	−0.527 509
0.3			−0.729 469	−0.545 828
0.4			−0.812 939	−0.565 435
0.5	−0.882 20	−0.584 88	−0.887 010	−0.585 714
1	−1.177 75	−0.687 72	−1.179 549	−0.687 943
2	−1.593 89	−0.872 63	−1.597 000	−0.872 647
3			−1.914 139	−1.031 356
4			−2.181 917	−1.171 360
5	−2.417 43	−1.297 88	−2.417 984	−1.297 884
10	−3.344 46	−1.810 06	−3.344 542	−1.810 074

Table 2 Numerical values of $-\theta'(0)$ and $-\phi'(0)$ for different values of Re, β_1, Pr, and Le, and $M = 0$

Re	β_1	Pr	Le	$-\theta'(0)$	$-\phi'(0)$
1	0.1	4.5	2	1.122 190	1.624 961
2				1.110 453	1.613 206
3				1.098 944	1.601 671
4				1.087 626	1.590 307
1	0.1	4.5	2	0.474 278	
	0.2			0.718 912	
	0.3			0.904 159	
	0.4			1.059 115	
1	0.1	1	2		1.221 940
		2			1.624 961
		3			2.008 637
		4			2.331 290
1	0.1	4.5	1	1.129 003	1.624 961
			2	1.533 036	2.219 778
			3	1.842 840	2.667 455
			4	2.103 945	3.037 788

5 Conclusion remarks

The following conclusions are noted in the analysis of swirling flow of the Maxwell fluid over the stretchable cylinder under the assumption of axisymmetric flow. The magnetic field is applied in the radial direction. The phenomena of thermal and solutal energy transport are deliberated with the help of classical Fourier's and Fick's laws.

(i) Both swirl and axial velocities reduce and decay exponentially for higher values of the Reynolds number Re and fluid motion occurs only near the surface.

(ii) Higher values of Re also reduce the heat and mass transports in fluid motion.

(iii) The increasing values of the magnetic parameter M fall down the swirling motion of the fluid.

(iv) For $Re = 0$, the fluid motion occurs near the surface due to the only torsional motion of the cylinder, and the main forced convection mechanism for the transport of energy is diminished.

(v) Higher values of Maxwell parameter β_1 boost up the temperature and concentration distributions but decline the flow field.

References

[1] CRANE, L. J. Boundary layer flow due to a stretching cylinder. *ZAMP*, **26**, 619–622 (1975)

[2] WANG, C. Y. Free convection on a vertical stretching surface. *ZAMM*, **69**, 418–420 (1989)

[3] VAJRAVELU, K. Viscous flow over a nonlinearly stretching sheet. *Applied Mathematics and Computation*, **124**, 281–288 (2001)

[4] ARIEL, P. D. Axisymmetric flow of a second grade fluid past a stretching sheet. *International Journal of Engineering Science*, **39**, 529–553 (2001)

[5] FANG, T. and YAO, S. Viscous swirling flow over a stretching cylinder. *Chinese Physics Letters*, **28**, 114702 (2011)

[6] SPRAGUE, M. A. and WEIDMAN, P. D. Three-dimensional flow induced by torsional motion of a cylinder. *Fluid Dynamics Research*, **43**, 015501 (2011)

[7] SUBHASHINI, S. V., SUMATHI, R., and POP, I. Dual solutions in a thermal diffusive flow over a stretching sheet with variable thickness. *International Communications in Heat and Mass Transfer*, **48**, 61–66 (2013)

[8] MUKHOPADHYAY, S. MHD boundary layer flow and heat transfer over an exponentially stretching sheet embedded in a thermally stratified medium. *Alexandria Engineering Journal*, **52**, 259–265 (2013)

[9] DANDAPAT, B. S., SINGH, S. K., and MAITY, S. Thin film flow of bi-viscosity liquid over an unsteady stretching sheet: an analytical solution. *International Journal of Mechanical Sciences*, **130**, 367–374 (2017)

[10] AHMED, J., KHAN, M., and AHMAD, L. Transient thin film flow of nonlinear radiative Maxwell nanofluid over a rotating disk. *Physics Letters A*, **383**, 1300–1305 (2019)

[11] JAVED, M. F., KHAN, M. I., KHAN, N. B., MUHAMMAD, R., REHMAN, M., KHAN, S. W., and KHAN, T. A. Axisymmetric flow of Casson fluid by a swirling cylinder. *Results in Physics*, **9**, 1250–1255 (2018)

[12] WEIDMAN, P. D. Radial stagnation flow on a twisting cylinder. *Journal of Fluids Engineering*, **141**, 114502 (2019)

[13] SALMAN, B. H., MOHAMMED, H. A., and MUNISAMY, K. M. Characteristics of heat transfer and fluid flow in microtube and microchannel using conventional fluids and nanofluids: a review. *Renewable and Sustainable Energy Reviews*, **28**, 848–880 (2013)

[14] JAVED, T., ALI, N., ABBAS, Z., and SAJID, M. Flow of an Eyring-Powell non-Newtonian fluid over a stretching sheet. *Chemical Engineering Communications*, **200**(3), 327–336 (2013)

[15] SHI, Y. and TANG, G. H. Simulation of Newtonian and non-Newtonian rheology behavior of viscous fingering in channels by the lattice Boltzmann method. *Computers & Mathematics with Applications*, **68**, 1279–1291 (2014)

[16] SANDEEP, N. and MALVANDI, A. Enhanced heat transfer in liquid thin film flow of non-Newtonian nanofluids embedded with graphene nanoparticles. *Advanced Powder Technology*, **27**, 2448–2456 (2016)

[17] RASHIDI, M. M., BAGHERI, S., MOMONIAT, E., and FREIDOONIMEHR, N. Entropy analysis of convective MHD flow of third grade non-Newtonian fluid over a stretching sheet. *Ain Shams Engineering Journal*, **8**, 77–85 (2017)

[18] DEVAKAR, M., RAMESH, K., CHOUHAN, S., and RAJE, A. Fully developed flow of non-Newtonian fluids in a straight uniform square duct through porous medium. *Journal of the Association of Arab Universities for Basic and Applied Sciences*, **23**, 9–18 (2017)

[19] PICCHI, D., POESIO, P., ULLMANN, A., and BRAUNER, N. Characteristics of stratified flows of Newtonian/non-Newtonian shear-thinning fluids. *International Journal of Multiphase Flow*, **97**, 109–133 (2017)

[20] KHAN, M., AHMED, J., and AHMAD, L. Chemically reactive and radiative von Kármán swirling flow due to a rotating disk. *Applied Mathematics and Mechanics* (*English Edition*), **39**(9), 1295–1310 (2018) https://doi.org/10.1007/s10483-018-2368-9

[21] SUN, X., WANG, S., and ZHAO, M. Numerical solution of oscillatory flow of Maxwell fluid in a rectangular straight duct. *Applied Mathematics and Mechanics* (*English Edition*), **40**(11), 1647–1656 (2019) https://doi.org/10.1007/s10483-019-2535-6

[22] WAQAS, H., IMRAN, M., KHAN, S. U., SHEHZAD, S. A., and MERAJ, M. A. Slip flow of Maxwell viscoelasticity-based micropolar nanoparticles with porous medium: a numerical study. *Applied Mathematics and Mechanics* (*English Edition*), **40**(9), 1255–1268 (2019) https://doi.org/10.1007/s10483-019-2518-9